Hindawi
Advances in Civil Engineering
Volume 2020, Article ID 8876785, 14 pages
https://doi.org/10.1155/2020/8876785

Research Article

Experimental Investigation of the Mechanical Behavior of NC Linings in consideration of Voids and Lining Thinning

Zude Ding,[1] **Jincheng Wen**,[1] **Xiafei Ji**,[1] **Zhihua Ren**,[2] **and Sen Zhang**[2]

[1]*Faculty of Civil Engineering and Mechanics, Kunming University of Science and Technology, Kunming 650500, China*
[2]*Yunnan Institute of Highway Science and Technology, Kunming 650051, China*

Correspondence should be addressed to Zude Ding; dzdvsdt@163.com

Received 9 April 2020; Revised 10 May 2020; Accepted 3 June 2020; Published 25 June 2020

Academic Editor: Salvatore Grasso

The presence of voids or lining thinning directly affects the mechanical behavior of linings, and these defects threaten the safety of tunnel operation. In this study, a series of 1/5-scale model tests was used to investigate the mechanical behavior of normal concrete (NC) linings in consideration of voids and combined defects. Test results showed that the void and combined defects substantially reduced the load-bearing capacity and deformation properties of the linings. The inelastic mechanical behavior of the linings was also significantly affected by the defects. The effects of lining defects located at the spandrel were slightly weaker than those of lining defects located at the crown. As the void size or degree of combined defects increased, the tensile strain at the location of the lining defects also increased. Therefore, the defect position of the linings was easily damaged. The defects considerably reduced the overall deformation of the linings but increased the local deformation. The distribution of lining cracks was concentrated at the defect position. In addition, different failure characteristics of the lining were observed due to the differences in defects.

1. Introduction

In recent years, the construction of tunnels and underground projects has progressed considerably, especially in China. However, quality defects, such as voids behind the lining and insufficient lining thickness, are common in operating tunnels. These defects are due to many reasons, such as tunnel design level, construction level, and complex geological conditions. They directly affect the mechanical properties of the lining and lead to tunnel diseases, such as lining cracks and water leakage [1–3].

Many studies have been conducted on the detection technology, formation mechanism, and reinforcement treatment technology of tunnel diseases and defects [4–8]. Compared with lining diseases, lining quality defects, such as voids behind the lining, insufficient thickness, and insufficient concrete strength, are more difficult to identify. The hazards caused by hidden tunnel defects are also not sufficiently clear; thus, tunnel defects have gradually elicited considerable attention from researchers [9–23]. Wang et al. [14] studied the influence of voids on the internal forces of lining structures via numerical simulation. The results showed that voids significantly change the internal force distribution of the lining structure, and the effects of different positions on the internal forces of the lining differ. Lai et al. [15] and Zhang et al. [16] found that an increase in void range worsens the stress concentration of the lining and reduces the axial force of the lining. Meanwhile, the lining bending moment is significantly increased at the location of the voids, resulting in the deterioration of the structural stress state and structural safety. Leung et al. [17] conducted an experimental study on the influence of voids on the distribution of surrounding rock pressure. Meguid et al. [18] and Wang et al. [19] discovered that voids behind the lining cause corrosion on the tunnel lining surface, concrete deterioration, reduced lining load capacity, and even lining damage. Experimental studies by Ding et al. [20] showed that the effects of voids on the bearing capacity of reinforced concrete linings vary with void size, void location, load direction, and subgrade stiffness. Wang et al. [21], Zhang et al. [22], and Qin et al. [23] discovered that insufficient lining thickness directly reduces not only the section stiffness

of the lining structure in the local range but also the contact stress between the supporting structure and surrounding rocks, thereby resulting in decreased structural strength and rigidity.

These research results show that the internal force of the lining and the pressure distribution of surrounding rocks are changed by tunnel quality defects. In several cases, these defects may even damage the lining. However, existing research mainly evaluated the influence of defects on the internal force of the lining and the pressure of surrounding rocks. Most studies have focused on investigating the mechanical behavior in the elastic stage of the lining. Tunnel defects can cause lining damage under extreme conditions. Therefore, the ultimate load-bearing capacity and plastic behavior of linings with defects must be considered to determine the influence of defects on the mechanical behavior of linings. According to practical engineering experience, void formation often occurs due to insufficient lining thickness [24]. However, only a few reports are available about the influence of combined defects on the mechanical behavior of tunnel structures. Existing tests mostly use small-scale models, which often result in reliability problems due to the difficulty of having similar designs. Therefore, a series of large scale (1/5) model tests was used in the present study to analyze the bearing capacity, deformation performance, and failure mode of normal concrete (NC) linings on the basis of single and combined defects. This study provides a scientific rationale for the safety evaluation and treatment design of defective linings.

2. Experimental Design

2.1. Test Loading Device. A horizontal loading test device was used for the lining model test [25–27]. The device included a reaction steel support frame, electrohydraulic loading jacks, and an equivalent subgrade setup. The reaction frame was assembled using bolts with H-shaped steel members and had nine loading points on the inside. Nine electrohydraulic jacks with a maximum load of 300 kN were installed at the loading points inside the reaction frame; they can apply load to any part of the lining arch. When simulating a concentrated load, the jack at the loading position was used as the loading jack, and the eight other jacks were used to support the rubber plates to simulate the subgrade reaction. The void behind the lining was simulated by removing the rubber plates, and the void size was controlled by adjusting or removing the rubber plates at the corresponding position. Figure 1 shows the test conditions of the lining under vertical loading, which considers the void at the spandrel.

2.2. Lining Specimens. A deeply buried two-lane road tunnel in Western China was used as the research object. The tunnel lining detection data showed that many voids behind the lining, lining thinning, and other diseases, such as lining cracks and leakage, were present. The height and width of the mountain tunnel were 7.8 and 11.8 m, respectively. The object of the model test was the lining with the void and lining thinning defects buried in the grade IV surrounding

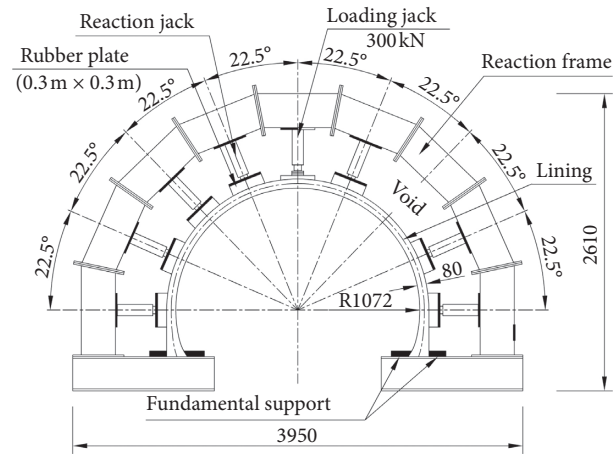

Figure 1: Experimental loading device (unit: mm).

rock, and the thickness of the lining was 0.4 m. A 1/5-scale model test was conducted in accordance with existing research [20, 27, 28]. This test used a concentrated load to simulate the case where the lining was subjected to loosening vertical soil pressure, horizontal plastic soil pressure, or unbalanced soil pressure, which was also similar to the loading method in previous literature [20, 27, 28]. A prototype material can be used for model tests when the influence of self-weight on the structure can be ignored and the external load is concentrated [29]. Therefore, we adopted prototype materials in our test. In addition, C25 ordinary concrete was utilized to create lining specimens, and Table 1 lists the mixing ratios. The compressive strength of the concrete at 28 days was 28.2 MPa. The lining specimens were made from the 1/5 scale of the prototype lining. The width, height, thickness, and longitudinal strength of the intact lining specimen were 2.3, 1.56, 0.08, and 0.3 m, respectively. The defect of lining thinning was achieved by reducing the thickness of the lining. Figure 2 shows a schematic of a lining specimen with insufficient thickness at the crown, photographs of the steel mold, and the test diagram. The lining specimens were prepared as follows: a set of steel molds was processed based on the size of the lining specimen, and the mold was assembled and fixed. A thin steel plate was placed and fixed on the thinned part of the mold, and the concrete was poured to form a lining specimen. The load test was carried out after 28 days of standard curing.

2.3. Simulation of the Surrounding Rock Restraint. Elastic rubber plates with a thickness of 10 cm were used to simulate artificial subgrade [28, 30]. The rubber plates combined with jacks were evenly mounted on the periphery of the lining to simulate the interaction between the lining and stratum (Figure 1). A uniaxial compression test was conducted to determine the elastic behavior of the rubber plate. Figure 3 shows the representative compression-deformation curves. As shown in this figure, the compression stiffness of the rubber plate was 3.38 MN/m when the compression-deformation was smaller than 20 mm. The Winkler elastic-foundation model assumes that the pressure at any point on

Table 1: Mix ratios of concrete (mass ratio).

Material	Cement	Fly ash	Fine aggregate	Coarse aggregate	Water	Water reducer
Normal concrete	1.0	0.18	2.53	3.6	0.54	0.006

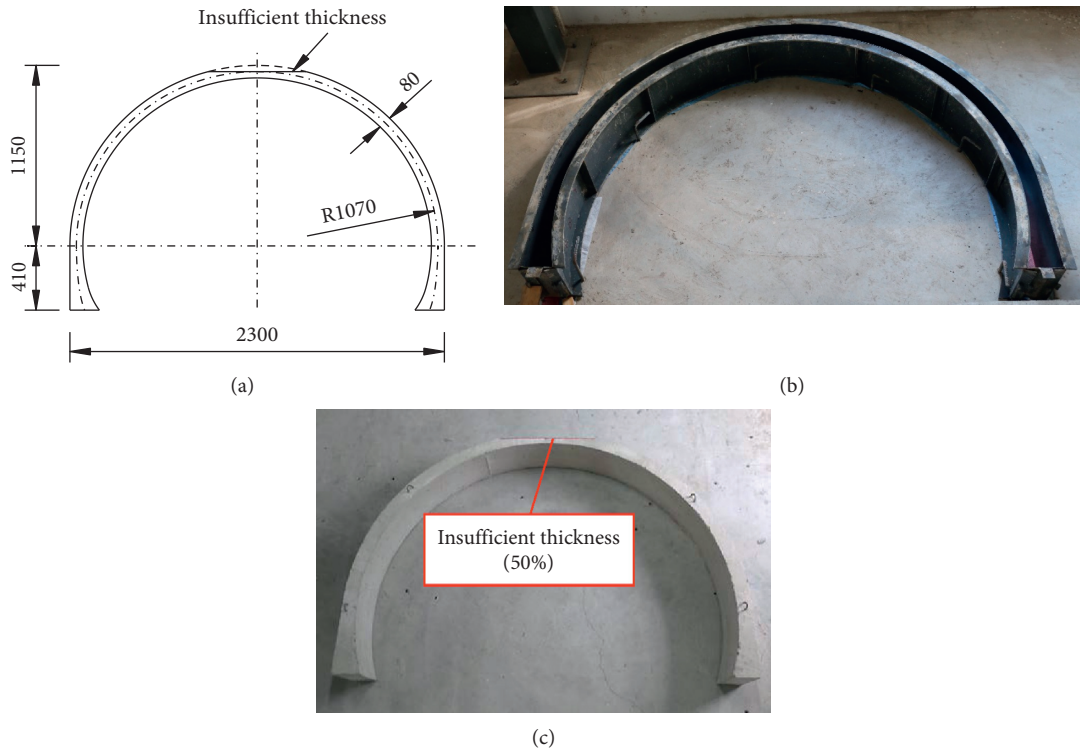

Figure 2: Lining specimen (unit: mm): (a) specimen geometry, (b) steel mold, and (c) lining specimen with thinning at the crown.

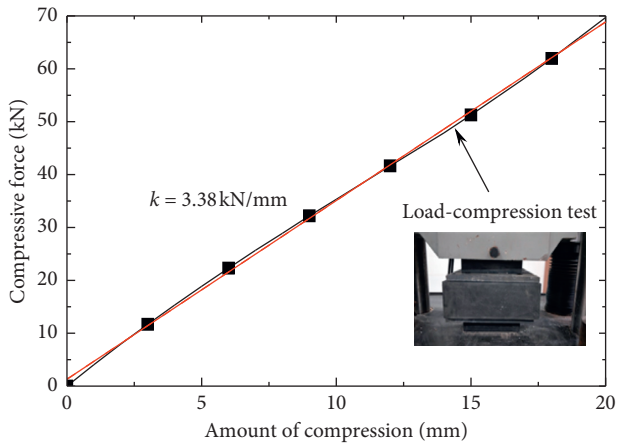

Figure 3: Compression-deformation curves of a rubber plate.

the foundation is proportional to the settlement, and the ratio is the subgrade stiffness. The equivalent coefficient of the subgrade reaction in the rubber plate constraint condition can be calculated as follows: $3.38 \times 8/3.23/0.3 = 27.9\ \mathrm{MN/m^3}$, where 3.38 MN/m is the compressive stiffness of a single rubber plate, 8 is the number of rubber plates, and 3.23 and 0.3 m are the constrained length and width of the lining specimen, respectively.

2.4. Model Test Cases. Voids behind the lining and lining thinning are regarded as typical quality defects of mountain tunnels in China. The presence of defects affects the load-bearing capacity of tunnel structures. Influencing factors, such as void location and size and the combination of void presence and lining thinning, were considered in the test to investigate the effects of quality defects on the mechanical properties of the linings. Two types of load directions, namely, vertical (90°) and oblique (45°) loads [29, 31], were used to simulate the loosening vertical and unbalanced soil pressures of the lining. The 45° oblique and 90° vertical loading modes were adopted for the cases where the defects are located at the crown (Figure 4(a)) and spandrel (Figure 4(b)), respectively. The void size was expressed using the angle α. The degree of lining thinning was expressed using the thickness reduction ratio δ:

$$\delta = \frac{(t_0 - t_1)}{t_0} \times 100\%, \tag{1}$$

where t_0 is the original lining thickness and t_1 is the thickness of the lining after thinning.

Ten model test conditions were considered, as shown in Table 2. A void is represented by the symbol "V" and its corresponding angle. Thinning is denoted by the symbol "T" and its corresponding thickness reduction ratio. For

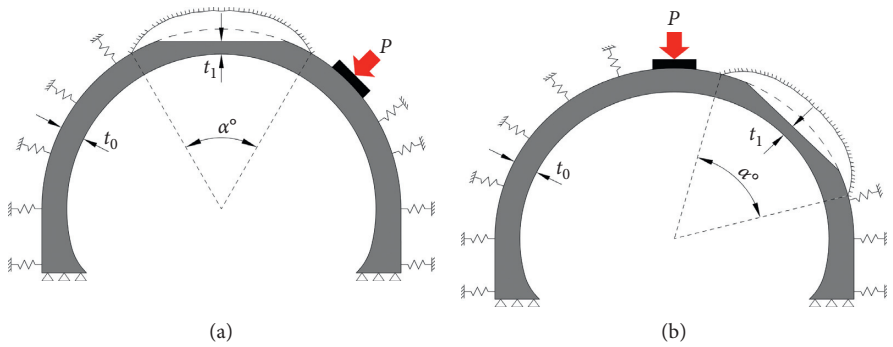

Figure 4: Model test case settings: (a) voids and thinning in the lining crown and (b) in the lining spandrel.

Table 2: Test conditions.

Serial number	Working condition	Load mode	Void		Thinning	
			Void location	Void size α (°)	Thinning location	Thinning ratio δ (%)
1	V0 (crown)	Oblique loading	Crown	0	Crown	0
2	V30 (crown)			30		0
3	V60 (crown)			60		0
4	V60T25 (crown)			60		25
5	V60T50 (crown)			60		50
6	V0 (spandrel)	Vertical loading	Spandrel	0	Spandrel	0
7	V60 (spandrel)			60		0
8	V180 (spandrel)			180		0
9	V30T25 (spandrel)			30		25
10	V60T50 (spandrel)			60		50

example, V30 represents a single defect with a void size of 30°, and V30T25 refers to combined defects with a void size of 30° and a thickness reduction ratio of 25%. Given that poor contact behind the lining is often accompanied by insufficient lining thickness [22], the conditions with only lining thinning defects did not exist in this test.

2.5. Sensor Arrangement. The load, displacement, and strain values during the loading process of the lining were collected by arranging pressure sensors, displacement transducers, and strain gauges, respectively. Figure 5 presents representative test arrangements under the vertical loading condition. Nine displacement measuring points were arranged on the inner side of the lining. The displacement of the lining at the crown was measured by a 5G106-type displacement transducer with a measuring range and accuracy of 300 and 0.01 mm, respectively. The displacements of the remaining positions were measured by a 5G105-type displacement transducer with a measuring range and accuracy of 100 and 0.01 mm, respectively. The inner and outer strains of the lining were measured by 30 resistance strain gauges. The concentrated load was measured by a 300 kN pressure sensor. The crack width was measured by a ZBL/F101-type crack meter during the experiment. The displacement control loading mode was adopted with a loading rate of 0.3–0.5 mm/min.

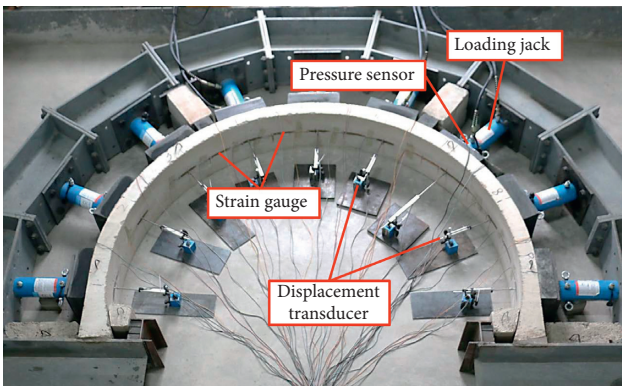

Figure 5: Test arrangements.

3. Experimental Results and Analysis

3.1. Effect of the Void on the Lining. Soundness (ζ) was used to evaluate the effect of existing defects on the load-bearing capacity of the lining as follows:

$$\zeta = \frac{P}{P_0} \times 100\%, \tag{2}$$

where P and P_0 are the peak load of the defective and intact linings, respectively. Table 3 presents the results obtained from the model test, where "crack load" and "displacement

Table 3: Main experimental results of lining specimens.

Serial number	Working condition	Crack load (kN)	Displacement at crack load (mm)	Peak load (kN)	Displacement at peak load (mm)	Soundness ζ (%)
1	V0 (crown)	11.15	2.3	61.15	39.3	100
2	V30 (crown)	10.94	2.0	32.73	30.4	53.5
3	V60 (crown)	9.32	1.0	15.30	1.7	25.0
4	V60T25 (crown)	8.31	1.0	12.71	1.4	20.8
5	V60T50 (crown)	8.20	0.9	12.17	1.4	19.9
6	V0 (spandrel)	11.24	2.1	53.81	54.1	100
7	V60 (spandrel)	7.90	1.5	34.34	14.0	63.8
8	V180 (spandrel)	5.67	1.0	7.04	2.5	13.1
9	V30T25 (spandrel)	9.32	1.3	30.40	9.9	56.5
10	V60T50 (spandrel)	7.70	1.2	17.23	5.6	32.0

at crack load" represent the load and the corresponding displacement of the loading point when the first crack of the lining appeared, respectively.

3.1.1. Load-Displacement Response. Figure 6 shows a significant difference in the load-displacement responses of the linings with different void sizes. This difference was mainly reflected in the three stages during the loading process (i.e., the elastic stage before cracking, the yield stage from crack load to peak load, and the failure stage after peak load). When the void size increased, the three stages of the load-displacement curve were not smooth, and the curve at the failure stage exhibited a steep drop. The void changed the shape of the load-displacement curve, reduced the load-bearing capacity of the lining, increased the brittleness of the lining, and affected the inelastic mechanical behavior of the lining.

When the void size at the crown increased from 0° to 60° (Figures 6(a), 7(a), and 8(a) and Table 3), the crack load of the lining decreased from 11.15 kN to 9.32 kN. The displacement at the crack load of the lining decreased from 2.3 mm to 1.0 mm, and the crack load and its displacement decreased by 16.4% and 56.5%, respectively. The peak load decreased from 61.15 kN to 15.3 kN, the displacement at the peak load decreased from 39.3 mm to 1.7 mm, and the reduction rates were 75% and 95.6%. When the void sizes were 30° and 60°, the soundness percentages of the lining were 53.5% and 25%, respectively. Therefore, as the void size increased, the lining was likely to crack, and its load-bearing and deformation capacities were significantly reduced. In particular, the lining was destroyed under a small load when the void size reached 60°.

Figures 6(b), 7(b), and 8(b) and Table 3 show that when the void size at the spandrel increased from 0° to 60°, the crack load of the lining decreased from 12.46 kN to 7.9 kN, the displacement at the crack load was reduced from 2.4 mm to 1.5 mm, and the crack load and its displacement decreased by 36.6% and 37.5%, respectively. The peak load decreased from 53.81 kN to 34.34 kN, the displacement at the peak load decreased from 54.1 mm to 14.0 mm, and the reduction rates were 36.2% and 74.1%. The test results indicated that the effect of the voids at the crown and spandrel on the load-displacement response of the lining was similar. When the lining completely lost the confinement of the surrounding rocks (i.e., the void size was 180°), the crack load and its displacement were 5.67 kN and 1.0 mm, which were 45.5% and 42.7% of the intact lining, respectively. The peak load and its displacements were 7.04 kN and 2.5 mm, which were only 13.1% and 4.6% of the intact lining, respectively; the soundness of the lining was 13.1%. These test results show that the load-bearing capacity of the lining was significantly reduced, and its deformation performance was basically lost. Therefore, the constraints of the surrounding rock significantly affected the mechanical response of the lining.

3.1.2. Secant Stiffness. The stiffness degradation of the lining components with voids was described by using secant stiffness (Figure 9) [32]. The change law of lining stiffness under different cases was similar to the increase in loading displacement, indicating that the decrement speed was high at first, slowed down, and finally stabilized. When the void size was large, the decay rate of secant stiffness was rapid, and the residual stiffness at the initial stage of loading was small. The residual stiffness of the lining was basically 0 when the void size at the crown and spandrel reached 60° and 180°, respectively. These results demonstrate that the void weakened the stability of lining stiffness.

3.1.3. Lining Strain. Figure 10(a) shows the strain-displacement curves of point A on the inside of the crown and point B on the outside of the crown. The variation in the compressive strain at point A differed under various void sizes. For the case with no void, the compressive strain at point A increased gradually with the increase in the early stage of loading displacement, rapidly increased after reaching a certain strain value, then gradually decreased and eventually became stable. For the cases with void sizes of 30° and 60°, the compressive strain at point A increased with the increase in loading displacement, and the curve shape changed smoothly. The change rule of the strain-displacement curve at point B was similar under different test conditions, indicating that an initial steady increase occurred, after which the curve shape increased rapidly after reaching a certain strain value. This phenomenon indicates that the lining crown cracked and was destroyed at this time. Under the same loading displacement, the tensile strain at point B increased with the increase in void size, whereas the loading displacement required to reach the critical tensile

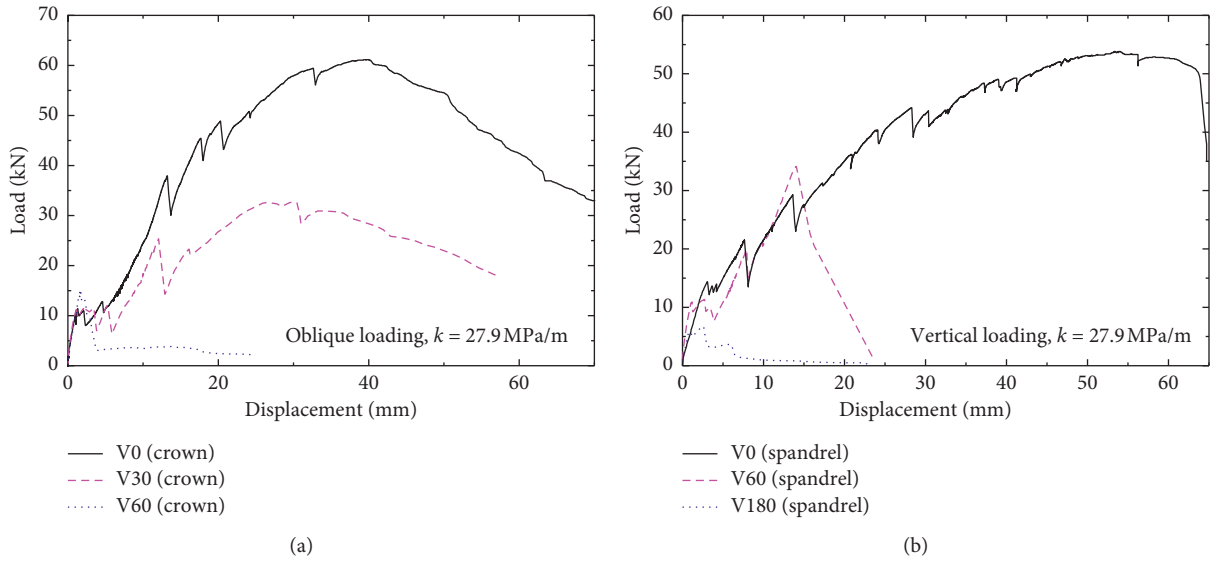

Figure 6: Load-displacement curves of the lining with void defects: (a) crown and (b) spandrel.

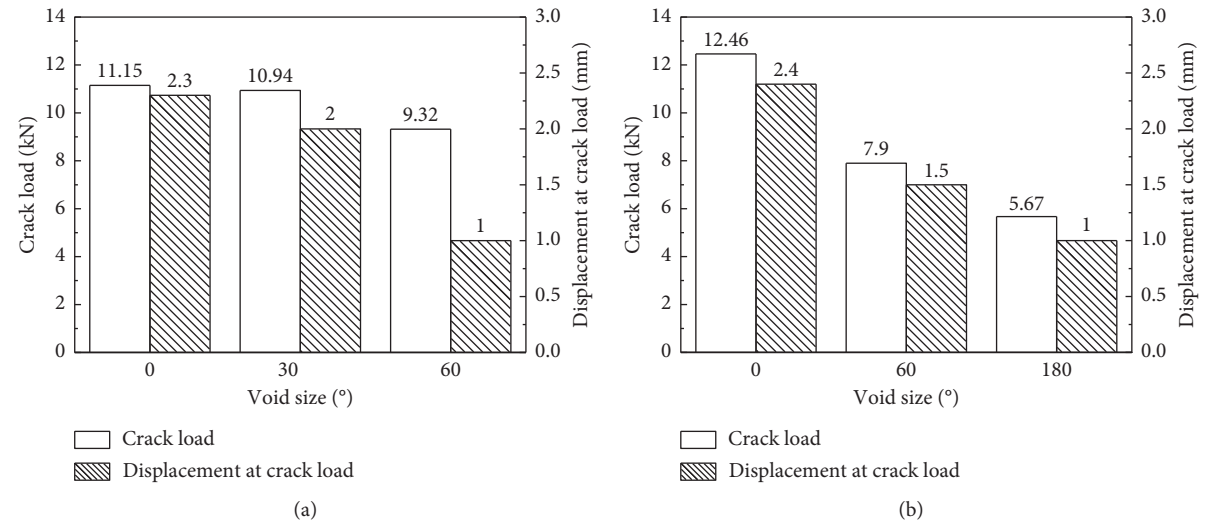

Figure 7: Crack load and the corresponding displacement of the lining with different void sizes: (a) crown and (b) spandrel.

strain (strain at the inflection position of the curve) decreased, indicating that the large tensile damage at the void caused lining failure to occur easily.

Figure 10(b) shows the strain-displacement curves of point C on the inside of the spandrel and point D on the outside of the spandrel. The change law of compressive strain at point C of the spandrel and point A of the crown was similar, indicating the inconsistent increase with the increase in void size. The change laws of tensile strain at point D and point B were consistent, exhibiting a two-stage development with the increase in loading displacement. However, the strain at point D increased more rapidly than the strain at point B. The tensile and compressive strain curves under the void size of 180° did not fail at the spandrel due to the location of the sensor arrangement.

3.1.4. Failure Mode of the Lining. Figures 11 and 12 show the crack, deformation analysis, and failure characteristics of the lining. "○" represents tensile cracks and "●" denotes the compression fracture.

Figure 11 shows that the cracks of the lining without void under the 45° oblique load were mainly distributed in the position of the loading point and its two sides near the crown and spring line. When the displacement loading was 2.3 mm, the first crack was observed inside the lining of the loading point, and the crack width was 0.2 mm. With an increase in displacement to 5.0 mm, the outer lining between the crown and left spandrel and between the right spandrel and right spring line began to crack, and the crack widths were 0.3 and 0.5 mm, respectively. The outer lining near the crown began to crack as the displacement increased further. The cracks

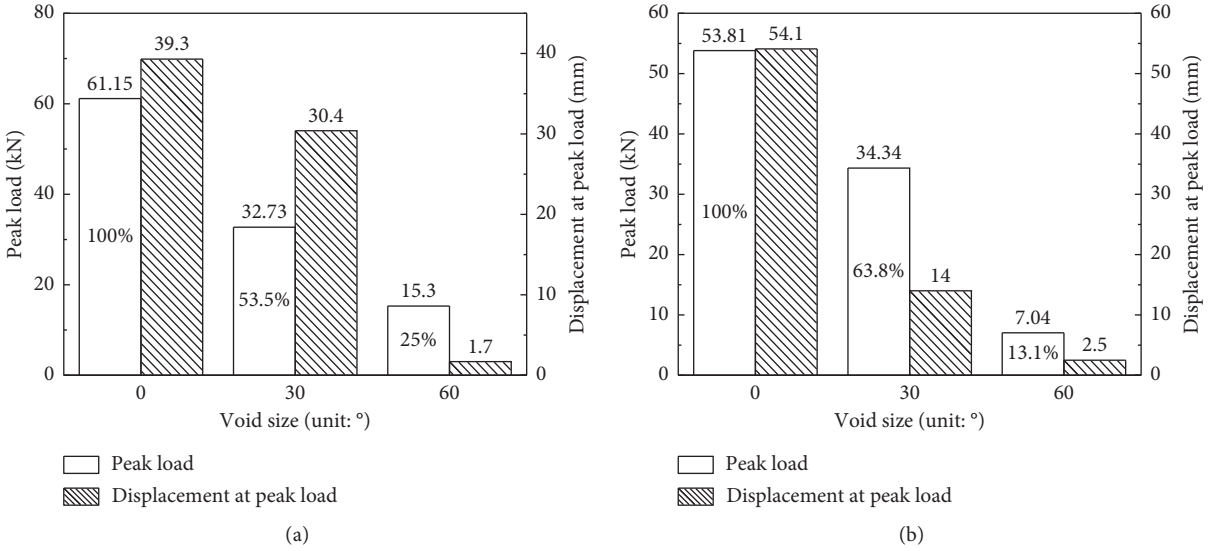

Figure 8: Peak load and the corresponding displacement of the lining with different void sizes: (a) crown and (b) spandrel.

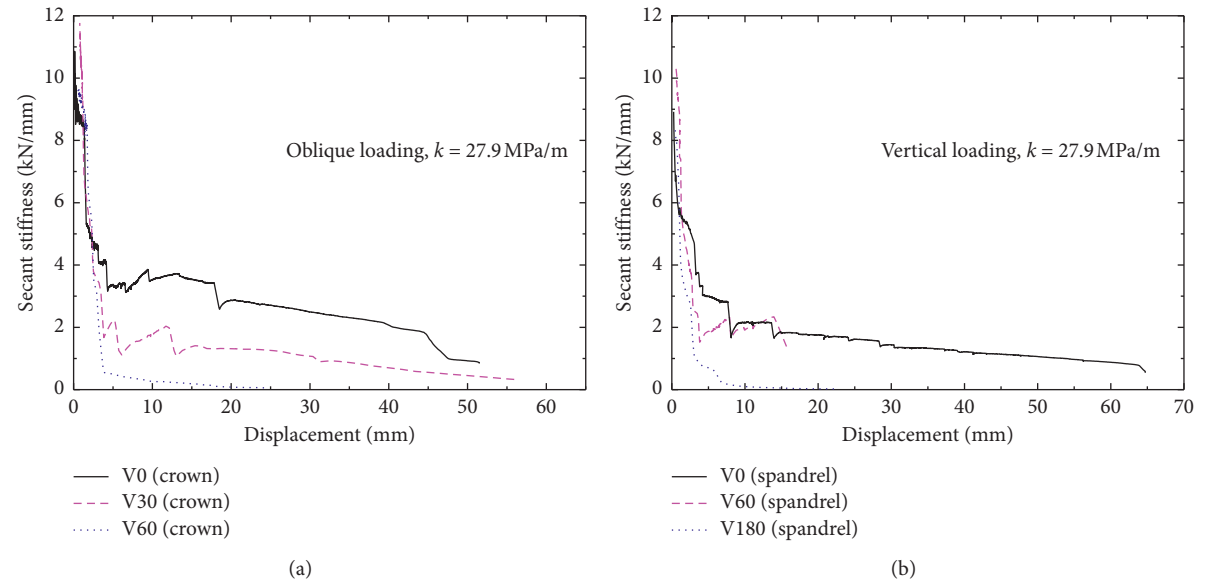

Figure 9: Secant stiffness-displacement curves of the lining with void defects: (a) crown and (b) spandrel.

expanded rapidly when the displacement exceeded 9.0 mm. Then, the lining was completely destroyed via concrete tensile rupture inside the right spandrel and concrete crushing near the crown and right spring line. This occurrence shows that the failure history of the lining was composed of crack initiation of the loading point section, formation of a plastic hinge, crack initiation of two sections on both sides of the loading point, development of three plastic hinges, and loss of the load-bearing capacity of the lining.

When a void existed at the crown, the failure modes of the linings were similar to those of the intact lining, but the crack distributions and developments were different. Take, for example, the void size of 60°. When the displacement loading was 1.0 mm, initial cracking was observed at the right spandrel, and tensile cracks at the crown and left spandrel were noted. The three main macrocracks expanded rapidly, and the lining was completely damaged by tension when the displacement loading was small. Concrete crushing was not observed in this case. With the increase in void size, the deformation performance was reduced and the brittle failure characteristics became increasingly evident. Except for those in the section of the loading point, the cracks were mainly distributed within the void range, indicating that the void range was the weak part of the lining.

Figure 12 shows that the deformation and cracks of the intact lining were distributed symmetrically under the vertical load. A tensile crack was first observed at the crown

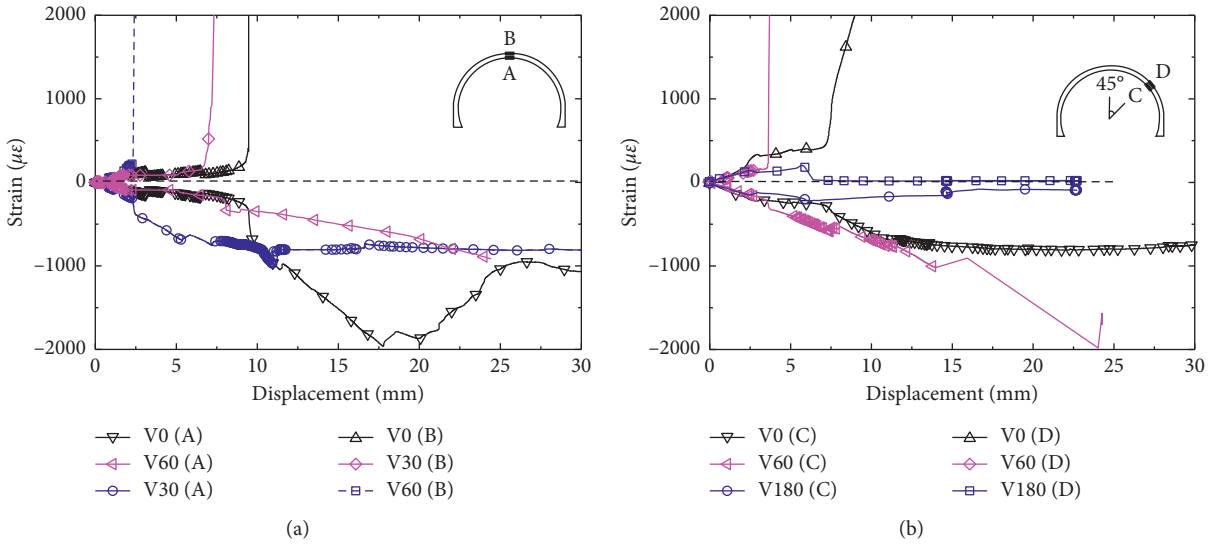

Figure 10: Strain-displacement curve of the lining with void: (a) crown and (b) spandrel.

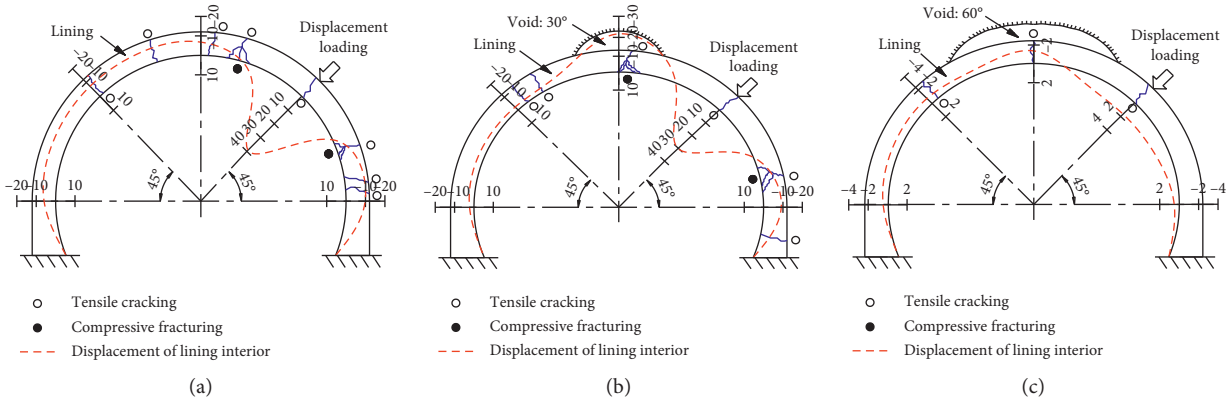

Figure 11: Distributions of the lining, cracking, and deformation at peak load (defects at the crown, displacement unit: mm): void sizes of (a) 0°, (b) 30°, and (c) 60°.

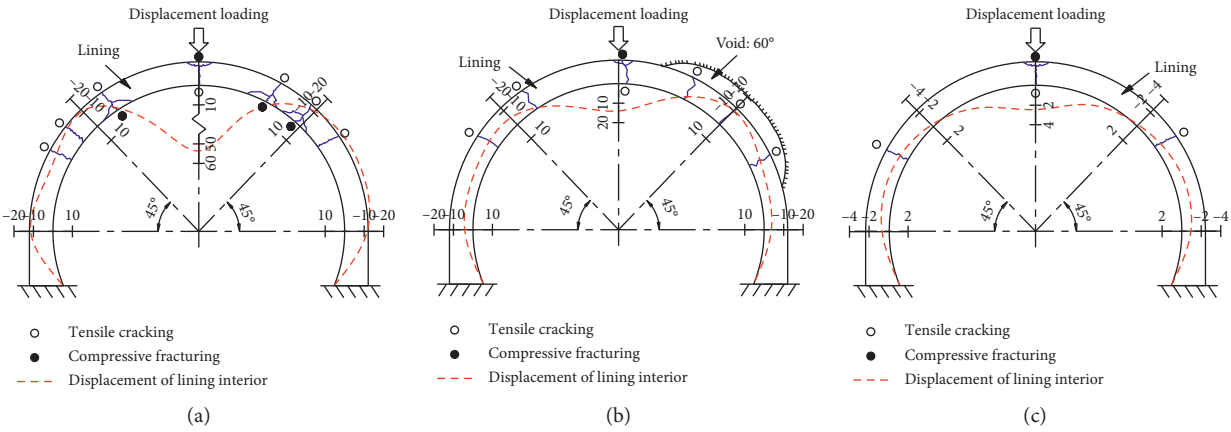

Figure 12: Distributions of the lining, cracking, and deformation at peak load (defects at spandrel, displacement unit: mm): void sizes of (a) 0°, (b) 60°, and (c) 180°.

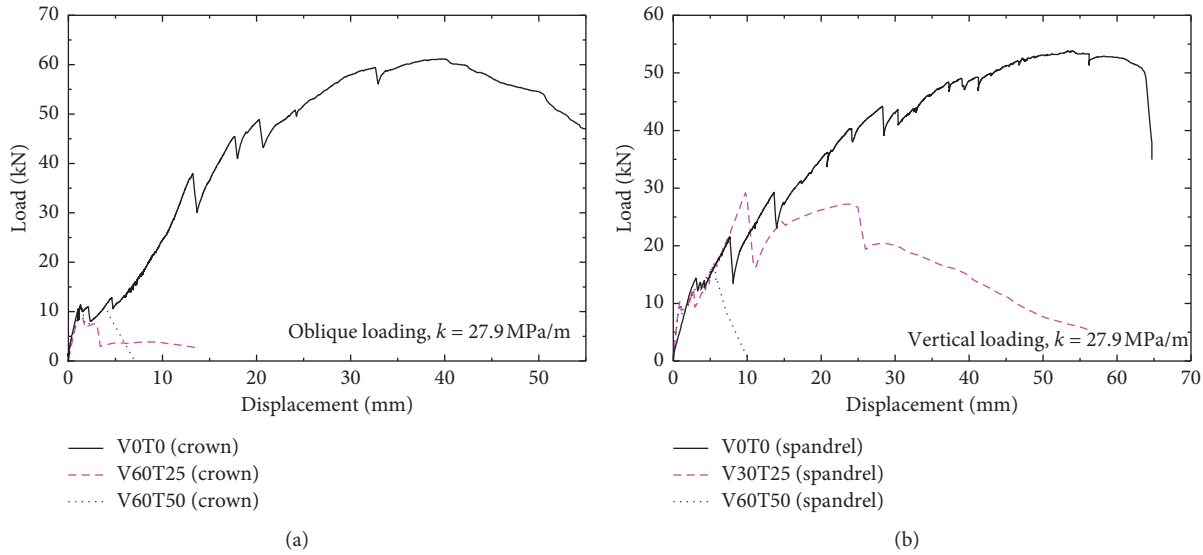

Figure 13: Load-displacement curves of the lining with combined defects: (a) crown and (b) spandrel.

when the displacement loading was 2.4 mm. The outer lining spandrels began to crack when the displacement increased to 5.0 mm. The cracks kept expanding gradually until the outside of the crowns and inside of the spandrels crushed, thereby forming plastic hinges.

Figure 12 also shows that when a void existed at the spandrel, the deformation and cracks of the lining were distributed asymmetrically in the axial direction and concentrated within the void range. The effects of the voids at the spandrel and crown on the mechanical behavior of the lining were similar. The displacement at failure load was reduced, and the brittleness was increased with the increase in void size. The weak part of the lining appeared in the void range. When the lining completely lost the confinement of the surrounding rocks, visible cracks appeared inside the crown when the displacement loading was only 1 mm; the cracks of the crown and spandrels expanded rapidly and penetrated through the lining when the displacement was 2.5 mm, thereby reaching the ultimate load-bearing capacity. Therefore, the presence of voids deteriorated the stress state of the lining and changed the deformation distributions and crack patterns of the lining.

3.2. Effect of Combined Defects on the Lining

3.2.1. Load-Displacement Response. Figure 13 shows the load-displacement response of the lining under different combined defect conditions. The load-displacement curve of the lining with combined defects was similar to that of the lining with void defects only. The three stages of the load-displacement curve were unclear when combined defects existed in the lining, and the boundary value of each stage decreased. As the degree of combined defects increased, the load-displacement curve of the lining presented sharp zigzag changes, and the mechanical properties of the lining were reduced significantly.

Figures 13(a)–15(a) and Table 3 show the experimental data of the lining with combined defects at the crown. Under the V60T25 condition, the crack load and displacement at the crack load were only 74.5% and 43.4%, respectively, whereas the peak load and displacement at the peak load were only 20.8% and 3.6%, respectively, compared with the intact lining. Under the V60T50 condition, the crack load and its corresponding displacement were only 73.5% and 39.1%, respectively, whereas the peak load and its corresponding displacement were only 19.9% and 3.6%, respectively, compared with the intact lining. Under these two conditions, the lining soundness was only around 20%, and the deformation capacity of the lining was basically lost. A comparison of V60T25 and V60T50 revealed that the load-bearing capacity of the lining was less affected by lining thinning. Meanwhile, lining thinning mainly affected the load-bearing and deformation capacities of the local part of the thickness. If the thinning part of the lining is loaded indirectly, then the thinning will have no significant effect on the load-bearing capacity of the lining.

Figures 13(b)–15(b) and Table 3 show the test results of the lining with combined defects at the spandrel. The load-displacement response of the lining with combined defects at the spandrel was similar to but slightly less than that of the lining with combined defects at the crown. With V30T25 as an example, the crack load and its corresponding displacement of the lining were 74.8% and 54.2%, respectively, whereas the peak load and its corresponding displacement were 56.5% and 18.3%, respectively, compared with the intact lining. Under the V60T25 condition, the lining crack load and its corresponding displacement were 61.8% and 50%, respectively, whereas the peak load and its corresponding displacement were 32% and 10.4%, respectively, compared with the intact lining. The soundness of the lining with defects at the spandrel was approximately 12% higher than that of the lining with defects at the crown under the same combined defects (V60T50). The presence of

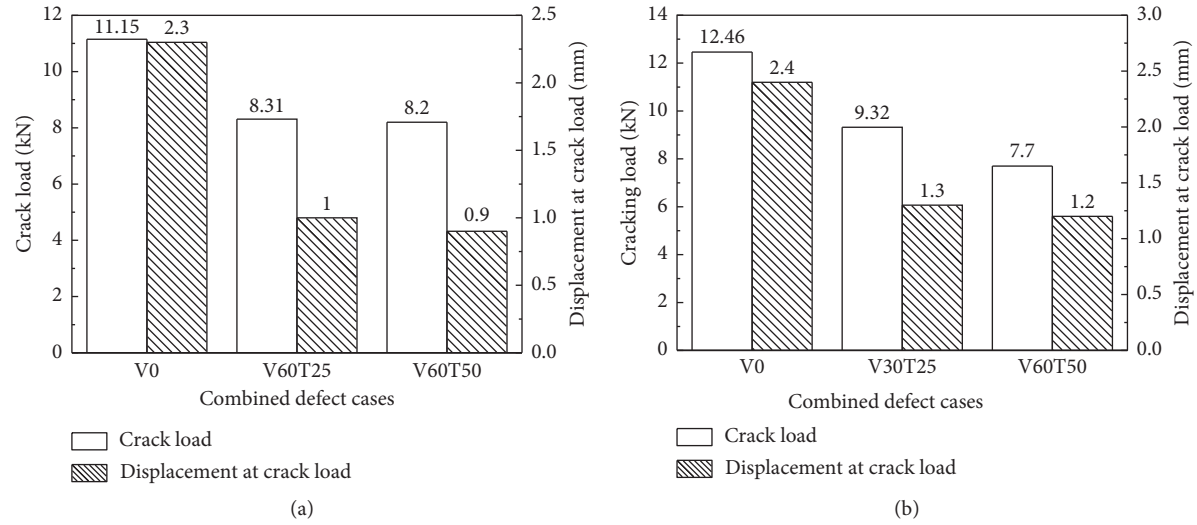

Figure 14: Crack load and displacement at the crack load of the lining with combined defects: (a) crown and (b) spandrel.

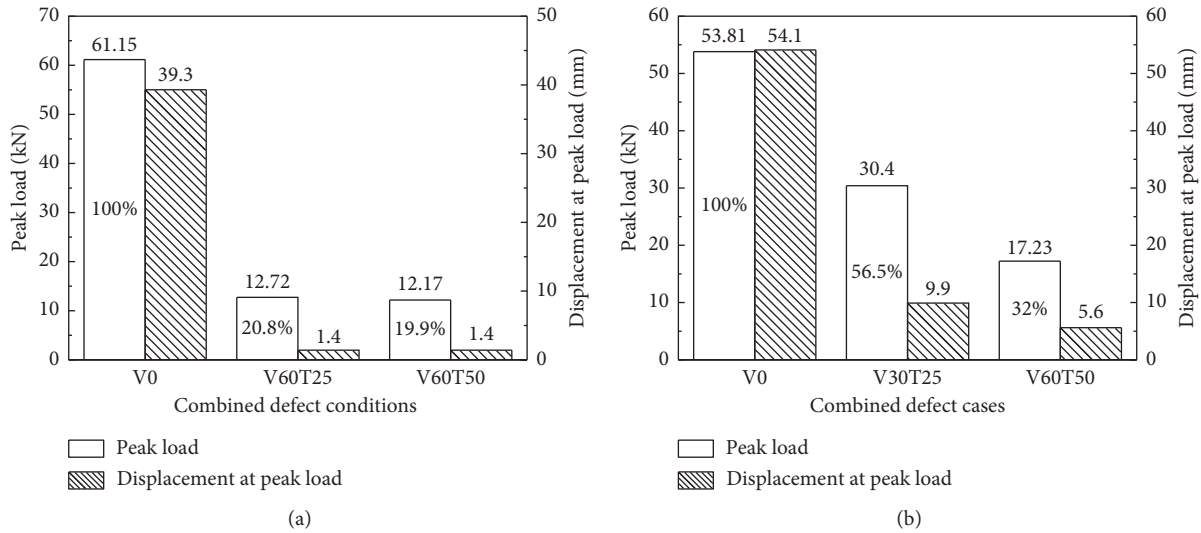

Figure 15: Peak load and displacement at the peak load of the lining with combined defects: (a) crown and (b) spandrel.

combined defects reduced the load-bearing capacity and deformation properties of the lining considerably regardless of the location of the defects.

3.2.2. Secant Stiffness. Figure 16(a) shows the secant stiffness-displacement curve of the lining with combined defects. The secant stiffness at the initial loading stage was relatively similar under different test conditions, and the influence of the combined defects was small. As the degree of combined defects increased, the stiffness decay rate of the lining increased, and the residual stiffness decreased, which was similar to the case of the lining with a single void defect. A comparison of the stiffness-displacement curves of the V60 (Figure 9(a)) and V60T25 (Figure 16(a)) conditions showed that the curve shapes of the two conditions were relatively close. The change in the secant stiffness was small under the two conditions, indicating that the stiffness of the lining was more affected by the void defect. Figure 16(b) shows that the stiffness-displacement curve of the V30T25 condition was similar to that of the intact lining, and their stiffness values were relatively close. When the defect range was small, the presence of defects did not affect the stiffness of the lining significantly. However, when the defect range was large (V60T50 condition), the stiffness stability of the lining was considerably impaired.

3.2.3. Lining Strain. Figure 17(a) shows that when a combined defect existed at the crown, the compressive strain of the lining inside the crown (point A) decreased, and the tensile strain growth rate increased outside the crown (point B). Moreover, the displacement required for the lining to

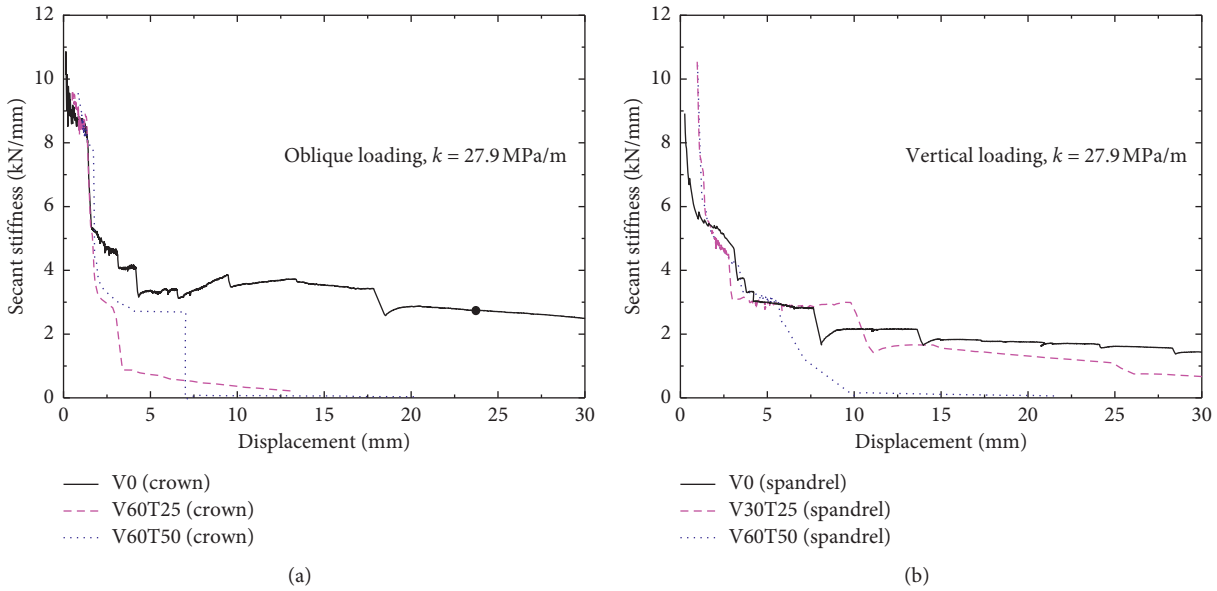

Figure 16: Secant stiffness-displacement curve of the lining with combined defects: (a) crown and (b) spandrel.

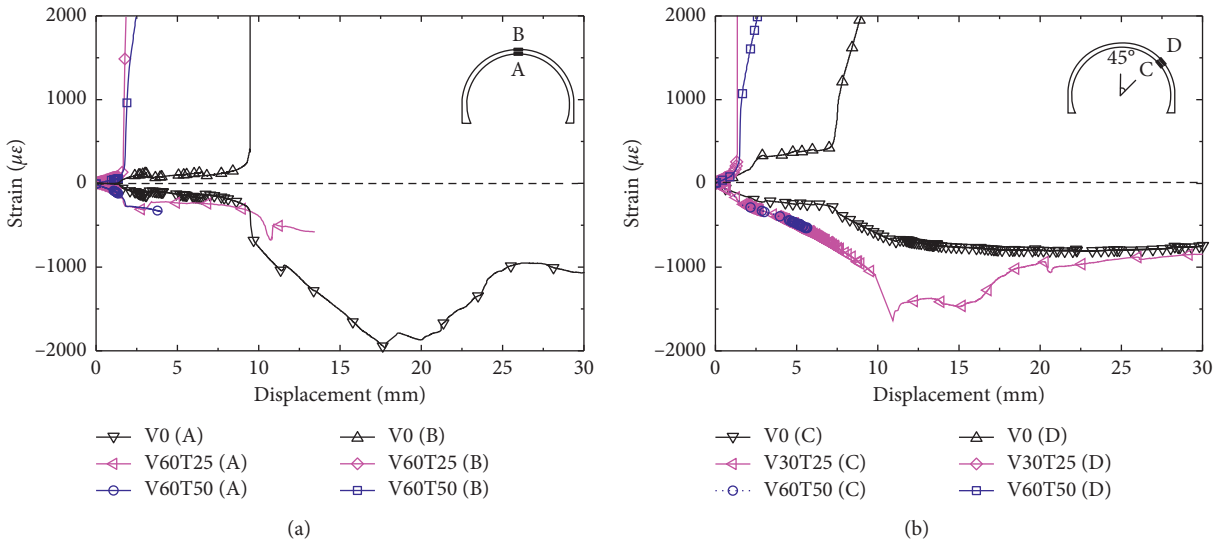

Figure 17: Strain-displacement curve of the lining with combined defects: (a) crown and (b) spandrel.

reach a steep strain increase was reduced significantly. These results show that the combined defects led to the increased eccentricity of the lining characterized by tensile failure. The tensile strain curves of the linings in the V60T25 and V60T50 conditions were similar to that of the lining in the V60 (void at the crown) condition. When the critical tensile strain was reached, the displacement of the two linings was slightly smaller than that in the V60 condition. The compressive strain curves of the two linings were significantly different from that in the V60 condition. Lining thinning considerably affected the compressive strain and slightly affected the tensile strain. When combined defects existed at the spandrel, the strain of the spandrel showed that the rates of compressive strain of point C and tensile strain of point D increased, and the strain-displacement curve shape was similar to that of the crown (Figure 17(b)).

3.2.4. Failure Mode of the Lining. Figure 18 shows the distribution of deformation and cracks of the lining with combined defects at the crown. The lining with combined defects reached the peak load and entered the failure stage under smaller deformation compared with the intact lining or the lining with a single defect. The deformation distribution of the linings was similar to that of the lining under the case of the void size 60° at the crown. However, this type of deformation concentrated on the defects was not as evident as that of the lining with a single defect. The crack

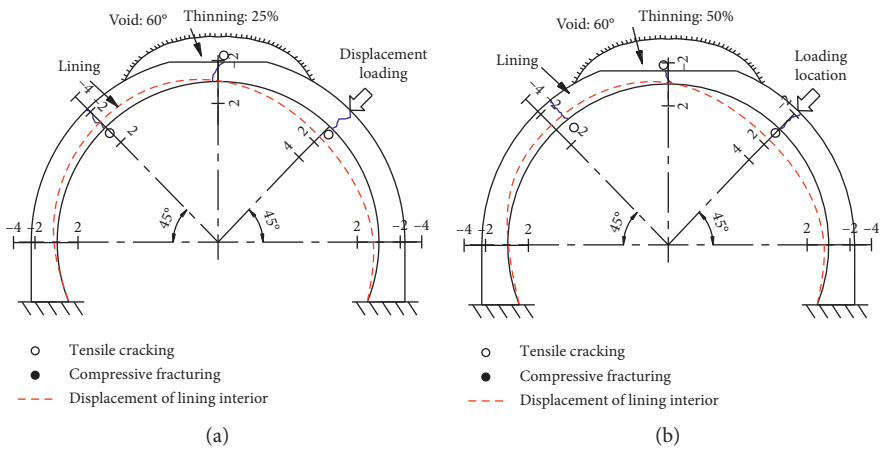

Figure 18: Distributions of lining cracking and deformation at the peak load (defects at the crown, displacement unit: mm): (a) V60T25 and (b) V60T50.

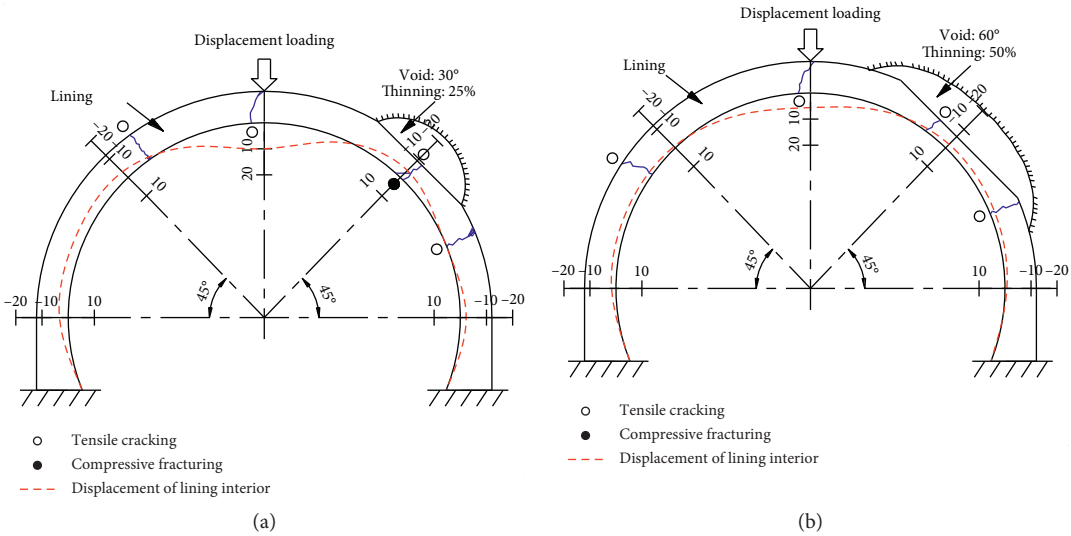

Figure 19: Distributions of lining cracking and deformation at the peak load (defects at spandrel, displacement unit: mm): (a) V30T25 and (b) V60T50.

distribution of the linings with combined defects at the crown was mainly located on the left and right spandrels and the crown. With V60T50 as an example, a macrocrack was observed initially in the right spandrel when the displacement loading was 0.9 mm, and a tensile crack with a 0.1 mm width in the crown was observed afterward when the displacement was 2.0 mm. When the displacement reached 3 and 5 mm, cracks appeared in the left spandrel and spring line, respectively, and the lining underwent complete failure. The main failure characteristics of the lining were tension failures, and no collapse phenomenon was observed.

Figure 19 shows the distribution of deformation and cracks of the lining with combined defects at the spandrel. The displacement at the peak load of the lining with combined defects at the spandrel was smaller than that of the intact lining. This phenomenon was consistent with the lining with combined defects at the crown, indicating that the presence of combined defects greatly decreased the lining deformation capacity. The cracks of the linings with combined defects at the spandrel were mainly distributed in the center and edge of the defect sections and crown. When the degree of defects was small (V60T25), the lining exhibited two failure characteristics, namely, tensile cracking and crushing. As the degree of defects increased, the lining only showed tensile damage, indicating that the failure characteristic of the lining was affected by the degree of defects. However, the failure mechanism of the lining can also be described by the formation and development of three plastic hinges, resulting in the loss of the overall load-bearing capacity of the lining.

4. Conclusions

A series of 1/5-scale model tests was performed to study the mechanical behavior of NC lining under the influence of

voids, lining thinning, and their combined defects. The main conclusions obtained based on the test results are as follows:

(1) The presence of defects changed the load-displacement response of the lining. The three stages of the load-displacement curve were unclear when the lining contained combined defects. The defects reduced the load-bearing capacity and deformation performance of the lining and affected the inelastic mechanical behavior of the lining.

(2) The initial secant stiffness of the lining was affected slightly by defects. Minor defects exhibited a slight effect on the secant stiffness of the lining. When the degree of defects was large, the lining stiffness decay rate was high, and the residual stiffness was small.

(3) Defects caused the lining tensile strain curve to increase early, making the lining easily susceptible to cracking. With the increase in the eccentricity of the lining, the main failure of the lining sections changed from compression failure to tensile failure. Thus, compressive strain generally showed an inconsistent growth with the increase in the degree of defects.

(4) The failure mode of the NC lining mainly showed the development of three plastic hinges and the loss of the overall load-bearing capacity of the lining. The presence of defects deteriorated the stress state of the lining. The deformation capacity of the lining was reduced, and the brittleness increased with the increase in the degree of defects. The range of defects was the weak part of the lining. The failure characteristics of the lining mainly displayed tensile cracking and compressive fracturing when the defect degree was small. When the degree of defects was large, the lining only showed tensile failure.

(5) Based on the analysis of the experimental results, the influence law of void defects and combined defects on the load-bearing capacity and deformation performance of the lining is obtained. The study can provide the theoretical and technical supports for the safety evaluation and treatment design of the linings with defects.

Data Availability

The data in figures and tables used to support the findings of this study are included within the article.

Conflicts of Interest

The authors declare no conflicts of interest.

Acknowledgments

The authors are grateful to the National Natural Science Foundation of China (No. 51768028) and the Transportation Science and Technology Project of Yunnan Province, China (No. 2016A01), for providing research funding.

References

[1] A. Inokuma and S. Inano, "Road tunnels in Japan: deterioration and countermeasures," *Tunnelling and Underground Space Technology*, vol. 11, no. 3, pp. 305–309, 1996.

[2] F. Huang, H. Zhu, Q. Xu, Y. Cai, and X. Zhuang, "The effect of weak interlayer on the failure pattern of rock mass around tunnel—scaled model tests and numerical analysis," *Tunnelling and Underground Space Technology*, vol. 35, pp. 207–218, 2013.

[3] N. Yasuda, K. Tsukada, and T. Asakura, "Three-dimensional seismic response of a cylindrical tunnel with voids behind the lining," *Tunnelling and Underground Space Technology*, vol. 84, pp. 399–412, 2019.

[4] E. W. H. N. C. Van, J. W. Sip, and F. P. Haring, "Design of repair measures of a damaged shield driven tunnel," *Tunnelling and Underground Space Technology*, vol. 21, no. 3, pp. 338-339, 2006.

[5] X. Pintado and B. E. Barragán, "Homogeneity of self-compacting concretes used in tunnel strengthening—a case study," *Tunnelling and Underground Space Technology*, vol. 24, no. 6, pp. 647–653, 2009.

[6] Z. Qu, L. Bai, S. Q. An, F. R. Ju, and L. Liu, "Lining seam elimination algorithm and surface crack detection in concrete tunnel lining," *Journal of Electronic Imaging*, vol. 25, no. 6, pp. 1–17, 2016.

[7] T. T. Yu, A. X. Zhu, and Y. Y. Chen, "Efficient crack detection method for tunnel lining surface cracks based on infrared images," *Journal of Computing in Civil Engineering*, vol. 31, no. 3, pp. 1–11, 2017.

[8] Y. J. Wu, S. L. Huang, and H. Z. Shi, "Stability analysis of cracks in concrete lining structure of water conveyance tunnel," *Advances in Engineering Research*, vol. 143, pp. 1463–1468, 2017.

[9] R. N. Cao, M. Ma, and R. H. Liang, "Detecting the void behind the tunnel lining by impact-echo methods with different signal analysis approaches," *Applied Sciences-Basel*, vol. 9, no. 16, pp. 1–18, 2019.

[10] X. S. Deng, T. Du, Q. Yuan et al., "Tunnel lining thickness and voids detection by GPR," *Electronic Journal of Geotechnical Engineering*, vol. 20, no. 7, pp. 2019–2030, 2015.

[11] A. Lalagüe, M. A. Lebens, I. Hoff, and E. Grøv, "Detection of rockfall on a tunnel concrete lining with ground-penetrating radar (GPR)," *Rock Mechanics and Rock Engineering*, vol. 49, no. 7, pp. 2811–2823, 2016.

[12] S. Konishi, K. Kawakami, and M. Taguchi, "Inspection method with infrared thermometry for detect void in subway tunnel lining," *Procedia Engineering*, vol. 165, pp. 474–483, 2016.

[13] A. Afshani, K. Kawakami, S. Konishi, and H. Akagi, "Study of infrared thermal application for detecting defects within tunnel lining," *Tunnelling and Underground Space Technology*, vol. 86, pp. 186–197, 2019.

[14] W. Wang, S. C. Liao, P. Ding, and D. Z. Chen, "Analysis of tunnel defect characteristic caused by cavities behind lining," *Advanced Materials Research*, vol. 261–263, pp. 1265–1269, 2011.

[15] J. X. Lai, C. Liu, Z. Hu, X. Cao, and X. L. Wang, "Numerical analysis of the influence of a cavity behind the shield lining on the tunnel structure," *Modern Tunnelling Technology*, vol. 54, no. 3, pp. 126–134, 2017, in Chinese.

[16] X. Zhang, C. P. Zhang, G. Feng, and K. H. Han, "Experimental studies on effect of voids behind tunnel linings on progressive failure process of tunnel structures," *Chinese Journal of*

Geotechnical Engineering, vol. 39, no. 6, pp. 1137–1144, 2017, in Chinese.

[17] C. Leung and M. A. Meguid, "An experimental study of the effect of local contact loss on the earth pressure distribution on existing tunnel linings," *Tunnelling and Underground Space Technology*, vol. 26, no. 1, pp. 139–145, 2011.

[18] M. A. Meguid and H. K. Dang, "The effect of erosion voids on existing tunnel linings," *Tunnelling and Underground Space Technology*, vol. 24, no. 3, pp. 278–286, 2009.

[19] J. Wang, H. Huang, X. Xie, and A. Bobet, "Void-induced liner deformation and stress redistribution," *Tunnelling and Underground Space Technology*, vol. 40, pp. 263–276, 2014.

[20] Z. D. Ding, X. F. Ji, X. Q. Li, Z. H. Ren, and S. Zhang, "Influence of symmetric and asymmetric voids on mechanical behaviors of tunnel linings: model tests and numerical simulations," *Symmetry-Basel*, vol. 11, no. 6, pp. 1–19, 2019.

[21] B. Wang, T. B. Li, C. He, and J. She, "Model test of effect of lining thinning on tunnel structure bearing capacity," *Journal of the China Railway Science*, vol. 35, no. 2, pp. 106–114, 2013, in Chinese.

[22] C. P. Zhang, X. Zhang, G. Feng, and D. L. Zhang, "Influence of insufficient lining thickness on the safety of a tunnel structure," *Modern Tunnelling Technology*, vol. 54, no. 2, pp. 137–143, 2017, in Chinese.

[23] G. Qin, S. Cao, and F. Yang, "Effect of deficiencies in the tunnel crown thickness on pressure tunnels with post-tensioned concrete linings," *Advances in Civil Engineering*, vol. 2018, pp. 1–14, 2018.

[24] Z. D. Ding, B. Zhang, X. Q. Li, J. Huang, and L. M. Peng, "Shaking table tests for investigating the effect of void behind lining on the seismic responses of a tunnel," *Journal of Vibration and Shock*, vol. 37, no. 14, pp. 156–161, 2018, in Chinese.

[25] N. Okano, "Development of a testing machine with a large tunnel lining model," *Railway Technology Avalanche*, vol. 19, p. 110, 2007.

[26] Z. Ding, J. Fu, X. Li, and X. Ji, "Mechanical behavior and its influencing factors on engineered cementitious composite linings," *Advances in Materials Science and Engineering*, vol. 2019, Article ID 3979741, 15 pages, 2019.

[27] Z. D. Ding, J. C. Wen, X. Q. Li, J. Fu, and X. F. Ji, "Mechanical behavior of polyvinyl alcohol-engineered cementitious composites (PVA-ECC) tunnel linings subjected to vertical load," *Tunnelling and Underground Space Technology*, vol. 95, Article ID 103151, p. 10, 2020.

[28] K. Yashiro, R. Hirata, N. Okano, and Y. Kojima, "Study on deformation and failure behavior of mountain tunnel linings which consist of various materials," *Journal of Japan Society of Civil Engineers, Ser. F1 (Tunnel Engineering)*, vol. 71, no. 2, pp. 78–94, 2015.

[29] W. Yuan, *Similarity Theory and Static Model Test*, Southwest Jiaotong University Press, Shanghai, China, 1998, in Chinese.

[30] X. Huang, Y. Zhu, Z. Zhang, Y. Zhu, S. Wang, and Q. Zhuang, "Mechanical behaviour of segmental lining of a sub-rectangular shield tunnel under self-weight," *Tunnelling and Underground Space Technology*, vol. 74, pp. 131–144, 2018.

[31] W. He, Z. Wu, Y. Kojima, and T. Asakura, "Failure mechanism of deformed concrete tunnels subject to diagonally concentrated loads," *Computer-Aided Civil and Infrastructure Engineering*, vol. 24, no. 6, pp. 416–431, 2009.

[32] G. Xu, B. Wu, D. Jia, X. Xu, and G. Yang, "Quasi-static tests of RC columns under variable axial forces and rotations," *Engineering Structures*, vol. 162, pp. 60–71, 2018.